A broad-spectrum substrate for the human UDP-glucuronosyltransferases and its use for investigating glucuronidation inhibitors

Zhou, Qi-Hang

2021-06-01

Zhou , Q-H , Qin , W-W , Finel , M , He , Q-Q , Tu , D-Z , Wang , C-R & Ge , G-B 2021 , ' A broad-spectrum substrate for the human UDP-glucuronosyltransferases and its use for investigating glucuronidation inhibitors ' , International Journal of Biological Macromolecules , vol. 180 , pp. 252-261 . https://doi.org/10.1016/j.ijbiomac.2021.03.073

http://hdl.handle.net/10138/341746
https://doi.org/10.1016/j.ijbiomac.2021.03.073

Research article

A broad-spectrum substrate for the human UDP-glucuronosyltransferases and its use for investigating glucuronidation inhibitors

Qi-Hang Zhou[a,1], Wei-Wei Qin[b,1], Moshe Finel[c], Qing-Qing He[a], Dong-Zhu Tu[a], Chao-Ran Wang[d], Guang-Bo Ge[a,*]

[a] *Institute of Interdisciplinary Integrative Medicine Research, Shanghai University of Traditional Chinese Medicine, Shanghai 201203, China.*

[b] *Department of Pharmacy, Huashan Hospital, Fudan University, Shanghai 200040, China*

[c] *Division of Pharmaceutical Chemistry and Technology, Faculty of Pharmacy, University of Helsinki, 00014, Finland*

[d] *Dalian Institute of Chemical Physics, Chinese Academy of Sciences, Dalian 116023, China*

* Corresponding author.

E-mail address: geguangbo@dicp.ac.cn (G.B. Ge)·

[1]These authors contributed equally to this work.

Abstract

Strong inhibition of the human UDP-glucuronosyltransferase enzymes (UGTs) may lead to undesirable effects, including hyperbilirubinaemia and drug/herb-drug interactions. Currently, there is no good way to examine the inhibitory effects and specificities of compounds toward all the important human UGTs, side-by-side and under identical conditions. Herein, we report a new, broad-spectrum substrate for human UGTs and its uses in screening and characterizing of UGT inhibitors. Following screening a variety of phenolic compound(s), we have found that methylophiopogonanone A (MOA) can be readily *O*-glucuronidated by all tested human UGTs, including the typical *N*-glucuronidating enzymes UGT1A4 and UGT2B10. MOA-*O*-glucuronidation yielded a single mono-*O*-glucuronide that was biosynthesized and purified for structural characterization and for constructing an LC-UV based MOA-*O*-glucuronidation activity assay, which was then used for investigating MOA-*O*-glucuronidation kinetics in recombinant human UGTs. The derived K_m values were crucial for selecting the most suitable assay conditions for assessing inhibitory potentials and specificity of test compound(s). Furthermore, the inhibitory effects and specificities of four known UGT inhibitors were reinvestigated by using MOA as the substrate for all tested UGTs. Collectively, MOA is a broad-spectrum substrate for the human UGTs, which offers a new and practical tool for assessing inhibitory effects and specificities of UGT inhibitors.

Key Words: Methylophiopogonanone A; UDP-glucuronosyltransferases (UGTs); Drug-drug interactions (DDI)

1. Introduction

Drug-metabolizing enzymes (DMEs) catalyze the detoxification and metabolic clearance of numerous endogenous substances (endobiotics) and xenobiotics, including drugs, carcinogens, environmental pollutants and food chemicals [1-5]. Strong inhibition of some key DMEs may significantly block the metabolic clearance of drugs or other toxins that are metabolized by the affected enzyme(s) to a meaningful degree, and thus leads to undesirable effects, including metabolic disorders or clinically relevant drug-drug or herb-drug interactions (DDIs or HDIs) [6-9]. As one of the most important class of phase II DMEs in humans, UDP-glucuronosyltransferases (UGTs) catalyze *O*-, *S*- or *N*-glucuronidation reactions of a large variety of lipophilic chemicals, including both endobiotics and xenobiotics. The biotransformation by UGTs generates more polar and water-soluble glucuronides that are easily excreted from the body *via* urine or bile [10, 11]. In most cases, the water-soluble glucuronides are biologically inactive or non-toxic, which makes UGTs as an important detoxification enzymes family in mammals.

In humans, over twenty different UGT enzymes have been identified, most of which are segregated into two subfamilies, 1A and 2B [12, 13]. These two UGT subfamilies include 18 UGT enzymes, but only 13 of them play currently-known roles in xenobiotics or and endobiotics metabolism. They are UGT1A1, -1A3, -1A4, -1A6, -1A7, -1A8, -1A9, -1A10, -2B4, -2B7, -2B10, -2B15, and -2B17, and they are available as commercial recombinant enzymes. The other 3 UGTs are UGT1A5, -2B11 and -2B28. It may be noted here that the activity of the commercial samples does not always accurately represent the activity of the enzyme in the native tissue [14]. The human UGTs tissue distribution, substrate spectra and biological functions in both endogenous compounds and xenobiotic metabolism have been extensively studied over the past few decades [13, 15].

Increasing amount of evidence has demonstrated that potent inhibition of human UGTs may profoundly slow-down their glucuronidation activities *in vivo* [16-18]. In turn, UGTs inhibition may bring some undesirable effects, including metabolic disorders such as hyperbilirubinemia [19, 20], or clinically relevant DDIs or HDIs [21-24].To reduce or even prevent the occurrence of clinically relevant DDIs, both the European Medicines Agency (EMA) and the United States (US) Food and Drug Administration (FDA) recommend that all

investigational new drugs should be assayed for their inhibitory potentials on a panel of human DMEs including cytochrome P450 enzymes (CYPs) and UGTs (such as UGT1A1 and UGT2B7), which play key roles in the detoxification and metabolic clearance of therapeutic drugs [25, 26]. A set of highly specific probe substrates for the human CYPs and carboxylesterases (CES) have been reported and are widely used for *in vitro* inhibition assays over the past few decades, which facilitate very well CYP/CES-mediated drug interaction studies [27-31]. By contrast, the approaches for assessing drug interaction potentials mediated by human UGTs are rarely reported, owing to the lack of a good substrate(s) for the entire panel of important human UGTs [32-34]. Currently, 4-methylumbelliferone (4-MU), a non-specific UGT substrate, is frequently used as the broad-spectrum substrate of human UGTs for evaluating UGT-mediated drug interaction potentials [35]. However, UGT1A4 and 2B10 do not catalyze 4-MU glucuronidation, while UGT2B4 and 2B17 catalyze this reaction at very low rates. Moreover, the K_m values for 4-MU glucuronidation by different human UGTs span roughly three orders of magnitude, ranging from 8.0 μM to 4204 μM [36]. These observations suggest that 4-MU is far from an ideal substrate for the human UGTs. Simultaneous assessment of the inhibitory potentials and specificity of a tested compound against human UGTs under identical conditions by using 4-MU as the substrate may yield misleading results. Therefore, better practical approaches for screening and characterization of inhibitors against a set of human UGTs are highly desirable.

This study reports a broad-spectrum substrate for the human UGTs and its applications for screening and characterization of UGT inhibitors, as well as for reinvestigating the specificity of known UGT inhibitors. Following screening a series of natural products bearing phenolic group(s), methylophiopogonanone A (MOA), a naturally occurring homoisoflavonoid, can be readily *O*-glucuronidated by all the tested human UGTs, including two typically *N*-glucuronidating enzymes (UGT1A4 and 2B10). MOA is *O*-glucuronidated by mammalian UGTs to generate a single and stable mono-*O*-glucuronide, which can be detected by liquid chromatography coupled with either a UV or mass spectrometry (MS) detector. We continued to biosynthesize and purify the *O*-glucuronide in order to determine its structure by NMR, since we wondered which of its two phenolic hydroxyls is conjugated by the enzymes. Subsequently, MOA-*O*-glucuronidation kinetics by the commercially available human UGTs,

liver and intestinal microsomes (HLM and HIM) were assayed. With the help of the purified MOA-*O*-glucuronide, we constructed an LC-UV based UGT inhibition assay and a standard curve for quantifying the formation rates of MOA-O-glucuronide. Such assay offers a practical approach for discovery and characterization of small-molecule inhibitors against human UGTs, while both the inhibition potency and the specificity of a tested compound against human UGTs can be assayed side-by-side under the same conditions.

2. Materials and Methods

2.1 Chemicals and Reagents

Methylophiopogonanone A, $MgCl_2$, nilotinib and magnolol were obtained from Meilun Biotechnology Co., LTD (Dalian, China). Tris and HCl were purchased from Sinopharm Chemical Reagent Co., Ltd (Shanghai, China). Polyethylene glycol hexadecyl ether (Brij 58), uridine 5'-diphosphoglucuronic acid (UDPGA) trisodium salt and dimethyl sulfoxide were obtained from Sigma-Aldrich (St. Louis, MO, USA). Amentoflavone was obtained from Chengdu Gelipu Biotechnology Co., Ltd (Sichuan, China). Fluconazole was purchased from Tokyo Chemical Industry Co., Ltd (Tokyo, Japan). Pooled human liver microsomes (HLMs, from 50 donors, Lot No. X008067), pooled human intestinal microsomes mixed gender (HIMs, Lot No. X02801) were purchased from BioreclamationIVT (Baltimore, MD, USA). The liver microsomes from different species including pooled male cynomolgus monkey (CyLM, Lot No. CYJC), pooled male New Zealand rabbit (RaLM, Lot No. LM-XBT-02M), pooled male ICR/CD-1 mouse (MLM, Lot No. STOM), pooled male Sprague-Dawley rat (RLM, Lot No. JPXY), pooled male beagle dog (DLM, Lot No. DMXD) and pooled male Yucatan minipig (PLM, Lot No. RUIB) were purchased from Research Institute for Liver Diseases (RILD, Shanghai, China). Human recombinant UGT isoforms (including 1A1, -1A3, -1A4, -1A6, -1A7, -1A8, -1A9, -1A10, -2B4, -2B7, -2B10, -2B15, -2B17) were obtained from Corning (NY, USA). Ultrapure water was prepared by a Millpore-Q water-purification system (Merck, Germany). All other reagents, such as acetonitrile, methanol and formic acid were of HPLC grade or of the highest grade commercially available.

2.2 UGT reaction phenotyping assays

A panel of human UGTs was used to assign the key UGTs that were responsible for

O-glucuronidation of the tested phenolic compounds [37, 38]. In brief, the incubation mixture (200 μL) consisted of Tris-HCl buffer (50 mM, pH 7.4), $MgCl_2$ (5 mM), human recombinant UGT (0.05 mg/ml) and each of tested compound (100 μM). After pre-incubation at 37℃ for 3 min, 10 μL UDPGA was added to start the reaction and the mixture was incubated for another 60 min, and then terminated by the addition of 200 μL ice-cold acetonitrile. The samples were vortexed and centrifuged at 20,000 × g for 20 min and the supernatants were subjected for LC-UV analysis.

2.3 Identification of MOA-*O*-glucuronide using UPLC/Q-TOF-MS

Identification of MOA and its *O*-glucuronide was conducted on an LC system (Shimadzu, Kyoto, Japan) coupled with a hybrid quadrupole orthogonal time-of-flight (Q-TOF) tandem mass spectrometer (AB Sciex, Darmstadt, Germany) equipped with an atmosphere pressure chemical ionization (ESI) ion source. The LC system was equipped with a SIL-20ACXR autosampler, a DGU-20AR vacuum degasser, two LC-20ADXR pumps and a CTO-20A column oven. Chromatographic separation was performed on a shim-pack VP-ODS column (4.6 μm, 150.0 mm × 2.1 mm, Shimadzu) at 40 ℃. The mobile phase consisted of 0.1% formic acid in ultrapure water (A) and acetonitrile (B), and the flow rate was 0.4 ml/min. The gradient elution was 20-80% B from 0.01-7.00 min, maintaining 80% from 7.00-7.5 min, 80-20% from 7.50-8.00 min, keeping 20% from 8.00-9.50 min.

Ionization of both MOA and MOA-*O*-glucuronide was operated under negative ion mode. Other parameters of the mass spectrometer were set as follows, Ion Spray Voltage (IS): -4500 V; Curtain Gas (CUR), nitrogen (35 psi), Collision Gas, medium; Ion Source Gas 1 (GS1): nitrogen (50 psi); Ion Source Gas 2 (GS2): nitrogen (50 psi), Temperature (TEM): 450 ℃. The Collision Energy (CE) and Declustering Potential (DP) for analytes were -10 V and -80 V, respectively. The MS data were recorded by AB Sciex Analyst Ver.1.6.3 software (AB Sciex, USA) and processed by Peak View software (AB Sciex, USA).

2.4 Biosynthesis, purification and structural characterization of MOAG

Before structural characterization and quantitative analysis, the *O*-glucuronide of MOA (MOAG) was biosynthesized and purified *via* reversed phase liquid chromatography (RPLC). MOAG was biosynthesized using rabbit liver microsomes (RaLM) as the enzyme source, since RaLM was easily available, inexpensive and displayed high conversion rate of MOA to

MOAG (**Figure 2**). Briefly, the incubation mixture (total volume 150 mL) was consisted of MOA (8.52 mg), Tris-HCl buffer (50 mM, pH 7.4), $MgCl_2$ (5 mM), Brij 58 (0.1 mg/mg protein), RaLM (0.8 mg/ml) and UDPGA (2 mM). After 5 min preincubation at 37 ℃, UDPGA was added to start the reaction. The reaction was terminated by adding ice-cold methanol (150 ml) after 6 h incubation at 37 ℃. Following centrifuged at 20,000 ×g, 4 ℃ for 20 min, the supernatant was collected, then evaporated and the precipitates were purified by a preparative HPLC system using a reversed-phase column. Finally, the obtained purified MOAG (8.0 mg, purity >98% as determined by LC-UV), as well as MOA, were dissolved in methanol-d4 for structural characterization using Bruker 400 nuclear magnetic resonance (NMR) spectrometer. The chemical shifts were recorded by ^{1}H NMR (400 MHz) and ^{13}C NMR (100 MHz), while tetramethylsilane (TMS) was used as the internal standard.

2.5 Quantification of MOA and its *O*-glucuronide by LC-UV

To quantify MOA and MOA 7-*O*-glucuronide (MOAG), a practical LC-UV based method was developed and validated. MOA and MOAG were analyzed by an LC system (Shimadzu, Japan) consisting of a CBM-20A system controller, two LC-30AD pumps, DGU-20A vacuum degasser, SIL-20AC auto-injector, SPD-M20A UV detector and a CTO-20AC column oven. A Shim-pack VP-ODS (4.6 μm, 150.0 mm × 2.1 mm, Shimadzu) analytical column was used to separate MOA and its *O*-glucuronide. The column temperature was maintained at 40 ℃. Acetonitrile (A) and water with 0.2% formic acid (B) were used as the mobile phase at a flow rate of 0.5 ml/min, and the gradient was as follow: 0.01-7.00 min, 80% B-20% B; 7.00-7.50 min, 20% B; 7.50-8.00 min, 20% B-80% B; 8.00-9.50 min, 80% B. The UV signals of MOA and its *O*-glucuronidation were recorded at 300 nm. A signal to noise (S/N) ratio of 3:1 was used to determine the limit of detection (LOD) of both MOA and MOAG. Calibration curves were constructed individually by plotting signal response *versus* the twelve known concentrations of MOA or MOAG. The inter-day and intra-day precision of this LC based method were also assessed by analyzing the standard solutions of MOA (3.42 ng) and MOAG (0.52 ng) within 24 h of three consecutive days. The overall precision was expressed using relative standard deviation (%, RSD). The stability of MOA and MOAG was determined by assaying samples before and after storage at 4 °C for 24 h or 48 h.

2.6 Enzymatic kinetic analyses

The catalytic efficacy and kinetic parameters of MOA-7-*O*-glucuronidation in HIM, HLM and 13 human recombinant UGTs were determined by using increasing concentrations of MOA (1-400 μM). Eadie-Hofstee plots, Michaelis-Menten equation and the substrate inhibition equation (Eq. A for Michaelis-Menten, and Eq. B for Substrate Inhibition) were used for fitting the substrate concentrations with MOA-*O*-glucuronidation rates. Model fitting and parameters estimation were performed by GraphPad Prism 7.0 software (GraphPad Software, Inc., CA, USA).

$$V = \frac{V_{max} \times [S]}{K_m + [S]} \quad \text{(A)}$$

$$V = \frac{V_{max} \times [S]}{S_{50} + [S](1 + \frac{[S]}{K_{si}})} \quad \text{(B)}$$

where V is the MOA-*O*-glucuronidation rate, V_{max} is the estimated maximum velocity, [S] is the substrate concentration, K_m or S_{50} is the concentration of substrate at which the reaction reaches the half of V_{max}, and K_{si} is the substrate inhibition constant.

For kinetic analyses, each point were tested at least three separate experiments, and the data are expressed as the mean ± SD (standard deviation). Kinetic parameters are reported as parameters and the error in the curve fitting.

2.7 Reinvestigation of the selectivity of known UGT inhibitors

The inhibitory effects of four known UGT inhibitors, amentoflavone, nilotinib, magnolol and fluconazole were reinvestigated by using MOA as the glucuronidation substrate. In brief, the incubation system (200 μL, total volume) contained $MgCl_2$ (5 mM), MOA, Tris-HCl buffer (50 mM, pH 7.4), a recombinant human UGT (protein concentrations are given in **Table S2**), and MOA in the absence or presence of either increasing concentration of amentoflavone (a broad-spectrum inhibitor of human UGTs), nilotinib (a specific inhibitor of UGT1A1), magnolol (a potent inhibitor of UGT1A7-10) and fluconazole (a specific inhibitor of UGT2B7) [39-43]. The concentrations of MOA were selected so that they will be below the K_m (S_{50}) value of MOA for the target UGT (**Table 2**). After 3 minutes preincubation at 37 ℃, the reaction was initiated by the addition of UDPGA (2 mM). The incubation times are shown in **Table S2**. The resulting concentrations of MOA and MOA 7-*O*-glucuronide were quantified by LC-UV as described above.

2.8 Statistical analysis

Except where otherwise noted, each point was tested in triplicate and all data were expressed as mean ± SD. The K_i and IC_{50} values were calculated by nonlinear regression analysis using GraphPad Prism 7.0 (GraphPad Software, Inc., La Jolla, USA).

3. Results and Discussion

3.1. Discovery and identification of a broad-spectrum substrate for human UGTs

To find a broad-spectrum substrate for the human UGTs, more than 20 compounds bearing phenolic group(s) have been collected and assayed for UGT reaction phenotyping, using a panel of the 13 commercial recombinant human UGTs. As shown in **Table S1**, each of the tested phenolic compounds can be *O*-glucuronidated by at least two human UGT enzymes, while UGT1A4 and UGT2B10 that are mainly known to catalyze *N*-glucuronidation activities [44, 45], displayed poor *O*-glucuronidation activities towards most, but not all of tested phenolic compounds. Notably, methylophiopogonanone A (MOA), a naturally occurring homoisoflavonoid, could be readily *O*-glucuronidated under physiological conditions (pH 7.4 at 37℃) by all the tested human UGTs, including UGT1A4 and UGT2B10. As depicted in **Figure 1 & Figure 3**, MOA could be readily catalyzed by each of the commercially available human UGTs, as well as by the liver preparations from both human and few other mammals, in the presence of UDPGA.

All the MOA glucuronidation reactions generated a single product peak (t_R = 4.74 min) which could be easily detected by liquid chromatography coupled with a UV or MS detector. The mass spectra of MOA and its product peak (under negative ion mode) are depicted in **Figures S1 and S2**. It is obvious that the quasi-molecular ion ($[M-H]^-$) of this product peak was *m/z* 517.1379, increasing *m/z* 176 compared with the substrate MOA, which indicating that this metabolite was a mono-*O*-glucuronide.[46, 47] Notably, this mono-glucuronide was not detected in the negative control incubations without either UDPGA, MOA or enzyme source (recombinant UGTs or microsomes), indicating that the formation of MOA-*O*-glucuronide (MOAG) is UDPGA- and UGT-dependent.

As far as we currently know, MOA is the first compound that is readily glucuronidated by all the main human UGTs, the enzymes that are known to metabolize drugs and some

endogenous compounds. Since the conjugation of MOA with a glucuronic acid from UDPGA appears to follow the same mechanism as common *O*-glucuronidation reactions (see below), the new discovery calls for further examination of the exact mechanism of *N*-glucuronidation reactions. However, in this first study on MOA glucuronidation we took a different direction. The first objective at this stage was to better characterize the glucuronide, not least since MOA has two phenolic hydroxyls and we were interested to know which of them is enzymatically conjugated. An important practical goal of this study was to establish how useful MOA is as a general substrate for the human UGTs, including relative rates and apparent affinity. The third and perhaps most applicable role of MOA-*O*-glucuronidation could be as a new and central tool in a method for screening and testing new compounds for their ability to inhibit any of the main human UGTs. To evaluate the degree of such inhibition, in order to estimate possible harmful effects from it. We have examined and develop this approach and validated its usefulness.

3.2 Biosynthesis, purification and identification of MOA-7-*O*-glucuronide

Considering that MOA bears two phenolic groups (at the C-5 and C-7 sites), it is necessary to reveal which of them accepts the glucuronic acid moiety in the UGT-catalyzed reaction. To this end, namely to determine the structure and glucuronidation site of MOA-*O*-glucuronide, the mono-glucuronide was biosynthesized using liver microsomes from animals as the enzyme sources. As shown in **Figure 2**, MOA could be readily *O*-glucuronidated by liver microsomes from different animal species, including monkey, minipig, rabbit, mouse, rat and dog. Among the tested liver microsomes, rabbit liver microsomes (RaLM) exhibited the highest conversion rate (>90%) under the same conditions and was then used for the biosynthesis of MOAG. Under the optimized conditions for MOAG biosynthesis by RaLM, MOAG was biosynthesized at high conversion rate and subsequently purified by a preparative HPLC system, using a reversed-phase column. Finally, 8.0 mg of MOAG (>98% purity) was obtained, with the total yield of both biosynthesis and purification (combined) was 62%.

Next, the chemical structure of MOAG was elucidated by ^{1}H NMR (600 MHz) and ^{13}C NMR (125 MHz), using the NMR data of the substrate (MOA) as the reference. The chemical shifts and NMR spectral signals for both MOA and MOAG were unambiguously assigned

and were listed in **Table 1**. As shown in **Table 1** and **Figures S3-S6**, in comparison with MOA, six additional glucuronic acid carbon signals (δ104.48, δ75.9, δ71.8, δ75.5, δ73.9, δ161.1) were observed, suggesting that a mono-glucuronic acid moiety was substituted in MOA. The ^{13}C-NMR spectrum of this metabolite showed that the signal of C-7 was shifted upfield (δ159.2), while the signals of C-6 and C-8 were shifted downfield (δ110.22 and δ111.69, for C-6 and C-8, respectively). Based on these findings, we inferred that the C-7 phenolic group (not the C-5 phenolic group) is the conjugation site. In addition, the results demonstrate that the glucuronic acid moiety of MOA-7-*O*-glucuronide is in *β*-D-configuration due to the featured chemical shift of G-1' (δ104.48) and the relatively large coupling constant of the anomeric proton (δ 7.7 Hz), which agrees well with the previous reports regarding *O*-glucuronides [47-50].

In this study we went deeper than many researchers and did not stop at finding a new compound that is glucuronidated by all the active UGTs. We biosynthesized relatively large amount of the product glucuronide and purified it, both at high efficiency. Then the structure of the glucuronide was solved by a combination of ^{1}H NMR and ^{13}C NMR, and the results clearly show that of the two phenolic hydroxyls, only the C-7 phenolic group is conjugated, while the C-5 phenolic group is not glucuronidated by human UGTs. It has been reported previously that mammalian UGTs exhibit different regio-selectivity or site preferences even among phenolic groups, such as ring A of hydroxy estrone and hydroxy estradiol, as well as the different phenolic groups on the ring A of flavones [51, 52]. The regioselective *O*-glucuronidation of the C-7 phenolic group can also be explained by the formation of an intramolecular hydrogen bond between the C-5 phenolic group and C-3 carbonyl group, which blocks the deprotonation of C-5 phenolic group (the first step for *O*-glucuronidation, a classic SN_2-reaction) and makes the hydrogen dissociation of the C-5 phenolic group more difficult than that of the C-7 phenolic group [53, 54]. For MOA, our findings also suggested that all tested human UGTs generate an identical mono-glucuronide and none appears to conjugate at the C-5 phenolic group of MOA.

3.3 Development of an LC-UV based MOA–*O*-glucuronidation activity assay

It is clearly visible in **Figure 2** that MOA (t_R = 6.74 min) and MOAG (t_R = 4.74 min) could be well-separated by an ODS column (see Methods for chromatography and gradient details).

The newly developed LC-UV based assay was fully validated in terms of specificity, sensitivity, linearity, precision and stability. As shown in **Figure 2**, most polar endogenous compounds in the UGT incubation samples could be eluted within the column dead-time while no interfering peak from endogenous matrix (such as HLM and recombinant human UGTs) was found around either MOA or MOAG. The limit of detection (LOD) and the limit of quantification (LOQ) were calculated as low as 0.09 ng, 0.45 ng and 0.11 ng, 0.42 ng for MOA and MOAG, respectively (**Table 3**). After that, the calibration curves for both MOA and MOAG were plotted, using increasing concentrations of purified MOA and MOAG (**Figure S7-S8**). As shown in **Fig. S7 & S8**, both MOA and MOAG exhibited excellent linearity (R^2=0.9996) between the peak areas and the concentrations within the ranges of 0.09-855.86 ng and 0.11-1295.86 ng, respectively. The intra-day and inter-day variabilities of this newly developed LC-UV assay were also investigated. As shown in **Table 3**, the relative standard deviation (RSD) for quantification of the two analytes was less than 1.0 % and 1.5 %, for MOA and MOAG, respectively. In addition, stability assay demonstrated that both MOA and MOAG are stable in the denaturation reaction mixture for 48 h (stored at 4℃). These findings suggest that the newly developed LC-UV based assay is reliable, sensitive, and suitable for measuring the rates of MOA glucuronidation, which provides a practical tool for assaying the kinetics of MOA glucuronidation by each of the 13 recombinant human UGTs. Meanwhile, such assay offers a practical approach for screening and characterization of small molecule inhibitors against the human UGTs, while both the inhibition potency and the specificity of a tested compound towards human UGTs can be assayed side-by-side under the same conditions.

3.4 Enzyme kinetics of MOA Glucuronidation by human UGT enzymes

The enzyme kinetics of MOA-7-*O*-glucuronide formation by HLM, HIM and 13 recombinant human UGTs was carefully investigated and the derived kinetic parameters are listed in **Table 2**. As seen in **Figure 4**, MOA-*O*-glucuronidation by HLM, HIM, UGT1A1, -1A3, -1A4, -1A6, -1A7, -2B4, -2B7, -2B10, -2B15 and -2B17 followed Michaelis-Menten kinetics, results that are also supported by linear Eadie-Hofstee plots. On the other hand, MOA-*O*-glucuronidation by UGT1A8, -1A9 and -1A10 displayed substrate inhibition kinetics.

All the tested human UGTs could catalyze MOA-*O*-glucuronidation at a relatively high catalytic efficacy, with the V_{max} values larger than or around 100 pmol/min/mg protein. Among all the tested UGT enzymes, UGT1A8 and UGT1A9 exhibited particularly high conversion rates, with V_{max} values of 2664 ± 694.4, and 1044 ± 289.7 pmol/min/mg protein, respectively. It may be noted, however, that direct correlation between the V_{max} value of the used recombinant UGT1A8 and the contribution of UGT1A8 in the native tissue, such as HIM, is far from clear and might differ largely, up to a gross overestimation of the true activity of intestinal UGT1A8 [14].

The K_m values that were derived from the kinetic assays suggest that the binding affinity of MOA is highest toward UGT1A1 (K_m = 4.69 ± 0.77 μM), followed by UGT2B7 (K_m = 8.72 ± 1.45 μM), UGT1A7 (K_m = 9.10 ± 1.13 μM), UGT2B4 (K_m = 9.69 ± 1.20 μM), and UGT1A10 (K_m = 10.37 ± 2.14 μM) (**Table 2**). As a result, UGT1A1 displayed the highest internal clearance (CL_{int}) for MOA (CL_{int} = 122.60 μL/min/mg protein), followed by UGT1A8 (CL_{int} = 86.61 μL/min/mg protein) and UGT1A9 (CL_{int} = 50.48 μL/min/mg protein).

The results with the recombinant UGTs are clear, but those from HLM and HIM should be looked at more carefully. HLM and HIM are not single enzymes, but mixtures of different UGTs that are expressed to different levels, and each of these UGTs has its own enzyme kinetics. With the exception of UGT1A9, many important hepatic UGTs, namely 1A1, 1A3, 1A4, 1A6, 2B4, 2B7, 2B10, 2B15 and 2B17 exhibited Michaelis-Menten kinetics in MOA glucuronidation (**Figure 4**). It is thus not surprising that HLM, too, displayed Michaelis-Menten kinetics. In the case of HIM the situation is somewhat more complicated since not that many UGTs are expressed in the small intestine, and their expression level is lower, explaining the lower V_{max} value. Assuming that there are only 4 UGTs that are expressed to considerable level [55], UGTs 1A1, 1A10, 2B7 and 2B17, then one of them, UGT1A10, displayed substrate inhibition kinetics (**Figure 4**) with rather high activity (**Table 2**) even if the low activity commercial enzyme was used. Hence, it seems that the HIM curve is a superposition of the high activity and low K_m value of UGT1A1 (Michaelis-Menten kinetics), high activity and quite low K_m value of UGT1A10 (substrate inhibition kinetics), quite low K_m value of UGT2B7 (Michaelis-Menten kinetics) that has a lower glucuronidation rate, and a high K_m value of UGT2B17 (Michaelis-Menten kinetics), that may compensate for

lower rate by higher expression level in HIM [56]. This superposition may explain the apparent Michaelis-Menten kinetics of HIM, but close look at the curve might reveal some traces of substrate inhibition on top of it (**Figure 4**).

The kinetic analyses demonstrated that MOA is a good substrate for the human UGTs, and this agent can be readily *O*-glucuronidated by all the tested human UGTs at a relatively high catalytic efficacy. This observation inspired us to test if it is feasible to use MOA as a molecular tool for simultaneous assessment of the inhibitory potentials and specificity of new compound(s) of interest toward the 13 human UGTs under identical incubation and analytical conditions.

3.5 Reinvestigation of the selectivity of four known UGT inhibitors

Following the findings described above, we used MOA to assess the inhibitory potentials of UGT inhibitors, starting by reinvestigating the selectivity of known UGT inhibitors. Four known UGT inhibitors, namely nilotinib (a specific inhibitor of the human UGT1A1), magnolol (a potent inhibitor of UGT1A7-UGT1A10), fluconazole (a specific inhibitor of the human UGT2B7) and amentoflavone (a potent broad-spectrum inhibitor of human UGTs), were selected for the study. As shown in **Figure 5** and **Table 4,** amentoflavone dose-dependently inhibited MOA glucuronidation in all the tested recombinant human UGTs. The results further revealed that among the tested 13 UGTs, amentoflavone is relatively a weak inhibitor against UGT2B10-catalyzed MOA-7-*O*-glucuronidation (IC_{50} = 37.4 μM), while it clearly exhibited stronger inhibition toward the other human UGTs, with IC_{50} values ranging between 0.26 ± 0.04 μM and 5.66 ± 1.78 μM (**Table 4**).

Nilotinib displayed potent inhibition of UGT1A1 (IC_{50} = 0.52 μM) and moderate inhibition of UGT1A3 and UGT1A4 (IC_{50} > 25 μM). These findings suggest that nilotinib is indeed a rather specific inhibitor of UGT1A1, at least if used at low concentrations. By contrast, magnolol displayed strong inhibition of UGT1A3, -1A4, -1A6 and -1A9 catalyzed MOA-7-*O*-glucuronidation (IC_{50} < 1 μM), as well as moderate inhibition of UGT1A1 and UGT1A10 catalyzing MOA-7-*O*-glucuronidation (IC_{50} > 20 μM) (**Figure 7**). These findings suggest that magnolol can strongly inhibit a panel of human UGT1As, and that its specificity as an inhibitor is somewhat different than previously assumed [41]. The last reinvestigated inhibitor in our set, fluconazole, only exhibited weak inhibition toward the human UGT2B7

(IC_{50} = 96.63 μM), which agrees well with the data in previous reports (shown in **Figure S9**) [42].

The reinvestigation of known UGT inhibitors provided us a very good validation for the new method, demonstrating that MOA is a good practical tool for simultaneous assessment of the inhibitory potentials and specificity of tested compounds against the recombinant UGTs that are most commonly used, under identical incubation and analytical conditions. Moreover, it allows extension of the spectrum of UGTs that are examined in such studies, as both the results of strong inhibition of UGT1A4-*O*-glucuronidation by magnolol and weak inhibition of this reaction by nilotinib (**Figures 6 and 7**). Hence, we not only re-approved the known inhibitions by these inhibitors, but also found that more UGTs than previously thought are sensitive to some of them.

4. Conclusion

In summary, this study reports the discovery of methylophiopogonanone A (MOA) as a novel broad-spectrum substrate for all the main human UGTs, including UGT1A4 and UGT2B10. Meanwhile, biosynthesis, purification and structural determination by NMR revealed that the MOA glucuronidation product is MOA-7-*O*-*β*-D-glucuronide. A practical LC-UV based method for UGT inhibition assays was developed by using MOA as a substrate. Following kinetic assays of MOA-*O*-glucuronidation by all the recombinant UGTs, this substrate was used for reinvestigating four known UGT inhibitors. The results demonstrated the suitability of the new method for screening UGT and analyzing inhibitors under identical assay conditions, as well as provided new insights into the inhibitor spectra of human UGTs. Collectively, MOA is a broad-spectrum substrate for human UGTs, which offers a practical tool for the discovery and characterization of potent or highly specific inhibitors of any important human UGT.

Acknowledgments

This work was supported by the NSF of China (81922070, 81703604, 81973286, 81773687), the National Key Research and Development Program of China

(2017YFC1700200, 2017YFC1702000), the Three-year Action Plan of Shanghai TCM Development (ZY-(2018-2020)-CCCX-5001), Shanghai Talent Development Fund (2019093), Program of Shanghai Academic/Technology Research Leader (18XD1403600), Shanghai Science and Technology Innovation Action Plans (20S21901500 & 20S21900900) supported by Shanghai Science and Technology Committee, and Shuguang Program (18SG40) supported by Shanghai Education Development Foundation and Shanghai Municipal Education Commission.

References

[1] L. Li, H. Hu, S. Xu, Q. Zhou, S. Zeng, Roles of UDP-glucuronosyltransferases in phytochemical metabolism of herbal medicines and the associated herb-drug interactions, Curr Drug Metab 13(5) (2012) 615-623.

[2] S.B. Kim, K.S. Kim, D.D. Kim, I.S. Yoon, Metabolic interactions of rosmarinic acid with human cytochrome P450 monooxygenases and uridine diphosphate glucuronosyltransferases, Biomed Pharmacother 110 (2019) 111-117.

[3] A.Z. DePriest, B.L. Puet, A.C. Holt, A. Roberts, E.J. Cone, Metabolism and Disposition of Prescription Opioids: A Review, Forensic Sci Rev 27(2) (2015) 115-145.

[4] C. Hou, W. Liu, Z. Liang, W. Han, J. Li, L. Ye, M. Liu, Z. Cai, J. Zhao, Y. Chen, S. Liu, L. Tang, UGT-mediated metabolism plays a dominant role in the pharmacokinetic behavior and the disposition of morusin in vivo and in vitro, J Pharm Biomed Anal 154 (2018) 339-353.

[5] M. Perreault, L. Gauthier-Landry, J. Trottier, M. Verreault, P. Caron, M. Finel, O. Barbier, The Human UDP-Glucuronosyltransferase UGT2A1 and UGT2A2 Enzymes Are Highly Active in Bile Acid Glucuronidation, Drug Metabolism and Disposition 41(9) (2013) 1616-1620.

[6] E. Kimoto, R.S. Obach, M.V.S. Varma, Identification and quantitation of enzyme and transporter contributions to hepatic clearance for the assessment of potential drug-drug interactions, Drug Metab Pharmacok 35(1) (2020) 18-29.

[7] M.A. Bahar, J. Kamp, S.D. Borgsteede, E. Hak, B. Wilffert, The impact of CYP2D6 mediated drug-drug interaction: a systematic review on a combination of metoprolol and paroxetine/fluoxetine, Brit J Clin Pharmaco 84(12) (2018) 2704-2715.

[8] Q.X. Zhong, Z.Q. Shi, L. Zhang, R.L. Zhong, Z. Xia, J. Wang, H. Wu, Y.T. Jiang, E. Sun, Y.J. Wei, L. Feng, Z.H. Zhang, D. Liu, J. Song, X.B. Jia, The potential of Epimedium koreanum Nakai for herb-drug interaction, J Pharm Pharmacol 69(10) (2017) 1398-1408.

[9] Q.H. Zhou, Y.D. Zhu, F. Zhang, Y.Q. Song, S.N. Jia, L. Zhu, S.Q. Fang, G.B. Ge, Interactions of drug-metabolizing enzymes with the Chinese herb Psoraleae Fructus, Chin J Nat Med 17(11) (2019) 858-870.

[10] A. Radominska-Pandya, P.J. Czernik, J.M. Little, E. Battaglia, P.I. Mackenzie, Structural and functional studies of UDP-glucuronosyltransferases, Drug Metab Rev 31(4) (1999) 817-899.

[11] M.B. Fisher, M.F. Paine, T.J. Strelevitz, S.A. Wrighton, The role of hepatic and extrahepatic UDP-glucuronosyltransferases in human drug metabolism, Drug Metabolism Reviews 33(3-4) (2001) 273-297.

[12] P.I. Mackenzie, K.W. Bock, B. Burchell, C. Guillemette, S. Ikushiro, T. Iyanagi, J.O. Miners, I.S. Owens, D.W. Nebert, Nomenclature update for the mammalian UDP glycosyltransferase (UGT) gene superfamily, Pharmacogenet Genomics 15(10) (2005) 677-685.

[13] A. Rowland, J.O. Miners, P.I. Mackenzie, The UDP-glucuronosyltransferases: Their role in drug metabolism and detoxification, Int J Biochem Cell B 45(6) (2013) 1121-1132.

[14] J. Troberg, E. Jarvinen, G.B. Ge, L. Yang, M. Finel, UGT1A10 Is a High Activity and Important Extrahepatic Enzyme: Why Has Its Role in Intestinal Glucuronidation Been Frequently Underestimated?, Mol Pharmaceut 14(9) (2017) 2875-2883.

[15] S. Oda, T. Fukami, T. Yokoi, M. Nakajima, A comprehensive review of UDP-glucuronosyltransferase and esterases for drug development, Drug Metab Pharmacok 30(1) (2015) 30-51.
[16] J. Vaillancourt, V. Turcotte, P. Caron, L. Villeneuve, L. Lacombe, F. Pouliot, E. Levesque, C. Guillemette, Glucuronidation of Abiraterone and Its Pharmacologically Active Metabolites by UGT1A4, Influence of Polymorphic Variants and Their Potential as Inhibitors of Steroid Glucuronidation, Drug Metabolism and Disposition 48(2) (2020) 75-84.
[17] L. Antonilli, V. Brusadin, M.S. Milella, F. Sobrero, A. Badiani, P. Nencini, In vivo chronic exposure to heroin or naltrexone selectively inhibits liver microsome formation of estradiol-3-glucuronide in the rat, Biochem Pharmacol 76(5) (2008) 672-679.
[18] F.F. Yang, C.Y. Ji, Z.Q. Cong, S.Q. Ma, C.Y. Liu, R.L. Pan, Q. Chang, Y.B. Ji, Y.H. Liao, Enhancing in vivo oral bioavailability of cajaninstilbene acid using UDP-glucuronosyl transferase inhibitory excipient containing self-microemulsion, Colloid Surface B 193 (2020).
[19] J. Meza-Junco, Q.S. Chu, O. Christensen, P. Rajagopalan, S. Das, R. Stefanyschyn, M.B. Sawyer, UGT1A1 polymorphism and hyperbilirubinemia in a patient who received sorafenib, Cancer Chemother Pharmacol 65(1) (2009) 1-4.
[20] J. Roy-Chowdhury, N. Roy-Chowdhury, I. Listowsky, A.W. Wolkoff, Drug- and Drug Abuse-Associated Hyperbilirubinemia: Experience With Atazanavir, Clin Pharmacol Drug Dev 6(2) (2017) 140-146.
[21] D. Kim, Y.F. Zheng, J.S. Min, J.B. Park, S.H. Bae, K.D. Yoon, Y.W. Chin, E. Oh, S.K. Bae, In vitro stereoselective inhibition of ginsenosides toward UDP-glucuronosyltransferase (UGT) isoforms, Toxicol Lett 259 (2016) 1-10.
[22] H. Qosa, B.R. Avaritt, N.R. Hartman, D.A. Volpe, In vitro UGT1A1 inhibition by tyrosine kinase inhibitors and association with drug-induced hyperbilirubinemia, Cancer Chemoth Pharm 82(5) (2018) 795-802.
[23] J.B. Park, D. Kim, J.S. Min, S. Jeong, D.Y. Cho, Y.F. Zheng, K.D. Yoon, S.K. Bae, Identification and characterization of in vitro inhibitors against UDP-glucuronosyltransferase 1A1 in uva-ursi extracts and evaluation of in vivo uva-ursi-drug interactions, Food Chem Toxicol 120 (2018) 651-661.
[24] J.O. Miners, N. Chau, A. Rowland, K. Burns, R.A. McKinnon, P.I. Mackenzie, G.T. Tucker, K.M. Knights, G. Kichenadasse, Inhibition of human UDP-glucuronosyltransferase enzymes by lapatinib, pazopanib, regorafenib and sorafenib: Implications for hyperbilirubinemia, Biochem Pharmacol 129 (2017) 85-95.
[25] FDA, In Vitro Metabolism- and Transporter- Mediated Drug-Drug Interaction StudiesGuidance for Industry, (2012).
[26] T.E.M. Agency, Guideline on the investigation of drug interactions, (2012).
[27] G.B. Ge, J. Ning, L.H. Hu, Z.R. Dai, J. Hou, Y.F. Cao, Z.W. Yu, C.Z. Ai, J.K. Gu, X.C. Ma, L. Yang, A highly selective probe for human cytochrome P450 3A4: isoform selectivity, kinetic characterization and its applications, Chem Commun 49(84) (2013) 9779-9781.
[28] S. Yamaori, N. Araki, M. Shionoiri, K. Ikehata, S. Kamijo, S. Ohmori, K. Watanabe, A Specific Probe Substrate for Evaluation of CYP4A11 Activity in Human Tissue Microsomes and a Highly Selective CYP4A11 Inhibitor: Luciferin-4A and Epalrestat, Journal of Pharmacology and Experimental Therapeutics 366(3) (2018) 446-457.
[29] J.J. Wu, G.B. Ge, Y.Q. He, P. Wang, Z.R. Dai, J. Ning, L.H. Hu, L. Yang, Gomisin A is a

Novel Isoform-Specific Probe for the Selective Sensing of Human Cytochrome P450 3A4 in Liver Microsomes and Living Cells, Aaps Journal 18(1) (2016) 134-145.
[30] J. Wang, E.T. Williams, J. Bourgea, Y.N. Wong, C.J. Patten, Characterization of Recombinant Human Carboxylesterases: Fluorescein Diacetate as a Probe Substrate for Human Carboxylesterase 2, Drug Metabolism and Disposition 39(8) (2011) 1329-1333.
[31] Z.H. Tian, L.L. Ding, K. Li, Y.Q. Song, T.Y. Dou, J. Hou, X.G. Tian, L. Feng, G.B. Ge, J.N. Cui, Rational Design of a Long-Wavelength Fluorescent Probe for Highly Selective Sensing of Carboxylesterase 1 in Living Systems, Anal Chem 91(9) (2019) 5638-5645.
[32] X. Lv, Y.L. Xia, M. Finel, J.J. Wu, G.B. Ge, L. Yang, Recent progress and challenges in screening and characterization of UGT1A1 inhibitors, Acta Pharm Sin B 9(2) (2019) 258-278.
[33] X. Lv, J.B. Zhang, J. Hou, T.Y. Dou, G.B. Ge, W.Z. Hu, L. Yang, Chemical Probes for Human UDP-Glucuronosyltransferases: A Comprehensive Review, Biotechnol J 14(1) (2019).
[34] M.T. Donato, S. Montero, J.V. Castell, M.J. Gomez-Lechon, A. Lahoz, Validated assay for studying activity profiles of human liver UGTs after drug exposure: inhibition and induction studies, Anal Bioanal Chem 396(6) (2010) 2251-2263.
[35] J.O. Miners, K.J. Lillywhite, A.P. Matthews, M.E. Jones, D.J. Birkett, Kinetic and inhibitor studies of 4-methylumbelliferone and 1-naphthol glucuronidation in human liver microsomes, Biochem Pharmacol 37(4) (1988) 665-671.
[36] V. Uchaipichat, P.I. Mackenzie, X.H. Guo, D. Gardner-Stephen, A. Galetin, J.B. Houston, J.O. Miners, Human udp-glucuronosyltransferases: isoform selectivity and kinetics of 4-methylumbelliferone and 1-naphthol glucuronidation, effects of organic solvents, and inhibition by diclofenac and probenecid, Drug Metab Dispos 32(4) (2004) 413-423.
[37] L. Zhu, G. Ge, Y. Liu, Z. Guo, C. Peng, F. Zhang, Y. Cao, J. Wu, Z. Fang, X. Liang, L. Yang, Characterization of UDP-glucuronosyltransferases involved in glucuronidation of diethylstilbestrol in human liver and intestine, Chem Res Toxicol 25(12) (2012) 2663-2669.
[38] Q.Q. He, Y. Chen, Q.H. Zhou, F. Zhang, Y.N. Wang, C.R. Wang, Y.Q. He, X.M. Liang, G.B. Ge, L. Yang, Deciphering the metabolic fates of a green fluorescent protein (GFP)-like fluorophore: Metabolite identification, isoenzyme contribution and species differences, Dyes Pigments 181 (2020).
[39] X. Lv, J.B. Zhang, X.X. Wang, W.Z. Hu, Y.S. Shi, S.W. Liu, D.C. Hao, W.D. Zhang, G.B. Ge, J. Hou, L. Yang, Amentoflavone is a potent broad-spectrum inhibitor of human UDP-glucuronosyltransferases, Chem-Biol Interact 284 (2018) 48-55.
[40] L. Ai, L. Zhu, L. Yang, G. Ge, Y. Cao, Y. Liu, Z. Fang, Y. Zhang, Selectivity for inhibition of nilotinib on the catalytic activity of human UDP-glucuronosyltransferases, Xenobiotica 44(4) (2014) 320-325.
[41] L. Zhu, G. Ge, Y. Liu, G. He, S. Liang, Z. Fang, P. Dong, Y. Cao, L. Yang, Potent and selective inhibition of magnolol on catalytic activities of UGT1A7 and 1A9, Xenobiotica 42(10) (2012) 1001-1008.
[42] V. Uchaipichat, L.K. Winner, P.I. Mackenzie, D.J. Elliot, J.A. Williams, J.O. Miners, Quantitative prediction of in vivo inhibitory interactions involving glucuronidated drugs from in vitro data: the effect of fluconazole on zidovudine glucuronidation, Br J Clin Pharmacol 61(4) (2006) 427-439.

[43] H. Xin, X.Y. Qi, J.J. Wu, X.X. Wang, Y. Li, J.Y. Hong, W. He, W. Xu, G.B. Ge, L. Yang, Assessment of the inhibition potential of Licochalcone A against human UDP-glucuronosyltransferases, Food Chem Toxicol 90 (2016) 112-122.
[44] S. Kaivosaari, M. Finel, M. Koskinen, N-glucuronidation of drugs and other xenobiotics by human and animal UDP-glucuronosyltransferases, Xenobiotica 41(8) (2011) 652-669.
[45] Y. Kato, T. Izukawa, S. Oda, T. Fukami, M. Finel, T. Yokoi, M. Nakajima, Human UDP-glucuronosyltransferase (UGT) 2B10 in drug N-glucuronidation: substrate screening and comparison with UGT1A3 and UGT1A4, Drug Metab Dispos 41(7) (2013) 1389-1397.
[46] M. Holcapek, L. Kolarova, M. Nobilis, High-performance liquid chromatography-tandem mass spectrometry in the identification and determination of phase I and phase II drug metabolites, Anal Bioanal Chem 391(1) (2008) 59-78.
[47] H. Xin, Y.L. Xia, J. Hou, P. Wang, W. He, L. Yang, G.B. Ge, W. Xu, Identification and characterization of human UDP-glucuronosyltransferases responsible for the in-vitro glucuronidation of arctigenin, J Pharm Pharmacol 67(12) (2015) 1673-1681.
[48] Y.L. Xia, S.C. Liang, L.L. Zhu, G.B. Ge, G.Y. He, J. Ning, X. Lv, X.C. Ma, L. Yang, S.L. Yang, Identification and characterization of human UDP-glucuronosyltransferases responsible for the glucuronidation of fraxetin, Drug Metab Pharmacokinet 29(2) (2014) 135-140.
[49] X. Lv, J. Hou, Y.L. Xia, J. Ning, G.Y. He, P. Wang, G.B. Ge, Z.L. Xiu, L. Yang, Glucuronidation of bavachinin by human tissues and expressed UGT enzymes: Identification of UGT1A1 and UGT1A8 as the major contributing enzymes, Drug Metab Pharmacok 30(5) (2015) 358-365.
[50] S.C. Liang, G.B. Ge, H.X. Liu, Y.Y. Zhang, L.M. Wang, J.W. Zhang, L. Yin, W. Li, Z.Z. Fang, J.J. Wu, G.H. Li, L. Yang, Identification and characterization of human UDP-glucuronosyltransferases responsible for the in vitro glucuronidation of daphnetin, Drug Metab Dispos 38(6) (2010) 973-980.
[51] J. Lepine, O. Bernard, M. Plante, B. Tetu, G. Pelletier, F. Labrie, A. Belanger, C. Guillemette, Specificity and regioselectivity of the conjugation of estradiol, estrone, and their catecholestrogen and methoxyestrogen metabolites by human uridine diphospho-glucuronosyltransferases expressed in endometrium, J Clin Endocr Metab 89(10) (2004) 5222-5232.
[52] C.Q. Hou, W.Q. Liu, Z. Liang, W.C. Han, J.Q. Li, L. Ye, M.H. Liu, Z. Cai, J. Zhao, Y. Chen, S.W. Liu, L. Tang, UGT-mediated metabolism plays a dominant role in the pharmacokinetic behavior and the disposition of morusin in vivo and in vitro, J Pharmaceut Biomed 154 (2018) 339-353.
[53] P. Wang, Y.L. Xia, Y. Yu, J.X. Lu, L.W. Zou, L. Feng, G.B. Ge, L. Yang, Design, synthesis and biological evaluation of esculetin derivatives as anti-tumour agents, Rsc Adv 5(66) (2015) 53477-53483.
[54] G.Y. He, S.X. Zhang, L. Xu, Y.L. Xia, P. Wang, S.Y. Li, L.L. Zhu, H.X. Xu, G.B. Ge, L. Yang, C-8 Mannich base derivatives of baicalein display improved glucuronidation stability: exploring the mechanism by experimentation and theoretical calculations, Rsc Adv 5(109) (2015) 89818-89826.
[55] T. Izukawa, M. Nakajima, R. Fujiwara, H. Yamanaka, T. Fukami, M. Takamiya, Y. Aoki, S. Ikushiro, T. Sakaki, T. Yokoi, Quantitative analysis of UDP-glucuronosyltransferase (UGT)

1A and UGT2B expression levels in human livers, Drug Metab Dispos 37(8) (2009) 1759-1768.
[56] Y. Sato, M. Nagata, K. Tetsuka, K. Tamura, A. Miyashita, A. Kawamura, T. Usui, Optimized Methods for Targeted Peptide-Based Quantification of Human Uridine 5 '-Diphosphate-Glucuronosyltransferases in Biological Specimens Using Liquid Chromatography-Tandem Mass Spectrometry, Drug Metabolism and Disposition 42(5) (2014) 885-889.

Figure and Table legends

Figure 1. Chemical structures and proposed mechanism of MOA and its 7-O-glucuronide.

Figure 2. Representative LC-UV profiles of MOA (tR = 6.74 min) and its 7-O-glucuronide (tR = 4.74 min) in liver microsomes from different animal species and negative control (without UDPGA, enzyme or MOA).

Figure 3. UGT reaction phenotyping assays of MOA 7-O-glucuronidation by using 13 various recombinant human UGT isoforms. Two substrate concentrations (10 μM & 100 μM) were used. Data expressed as mean ± SD (n=3).

Figure 4. Enzymatic kinetics of MOA-7-O-glucuronidation in HLM (A), HIM (B) or recombinant human UGT1A1 (C), -1A3 (D), -1A4 (E), -1A6 (F), -1A7 (G), -1A8 (H), -1A9 (I), -1A10 (J), -2B4 (K), -2B7 (L), 2B10 (M), -2B15 (N) and -2B17 (O). Eadie-Hofstee plots (V/S-V) are displayed as the insets. Data points represent the mean of triplicate independent determinations, while the error bars represent the calculated S.D.(n=3).

Figure 5. Dose-inhibition curves of amentoflavone against human UGT1A1 (A), -1A3 (B), -1A4 (C), -1A6 (D), -1A7 (E), -1A8 (F), -1A9 (G), -1A10 (H), -2B4 (I), -2B7 (J), 2B10 (K), -2B15 (L), -2B17 (M) and the positive control (sorafenib) against human UGT1A1 catalyzed MOA-7-*O*-glucuronidation. Data represent the mean ± SD (n=3).

Figure 6. Dose-inhibition curves of nilotinib against human UGT1A1 (A), -1A3 (B), -1A4 (C) and positive control (sorafenib) against human UGT1A1 catalyzed MOA-7-*O*-glucuronidation. Data represent the mean ± SD (n=3).

Figure 7. Dose-inhibition curves of magnolol against human UGT1A1 (A), -1A3 (B), -1A4 (C), -1A6 (D), -1A7 (E) and -1A10 (F) catalyzed MOA-7-*O*-glucuronidation. Data represent the mean ± SD (n=3).

Table 1. Assignment of the chemical shifts of each proton and carbon signals of MOA and its *O*-glucuronide.

Table 2. Kinetic parameters for MOA-7-*O*-glucuronidation in HLM, HIM and 13 recombinant human UGT enzymes.

Table 3. The linear range, LOD, Intra- and inter-day variability of the LC-UV based assay for quantitative determination of MOA and MOAG.

Table 4. IC_{50} values of four known UGT inhibitors against 13 human UGTs by using MOA as the substrate.

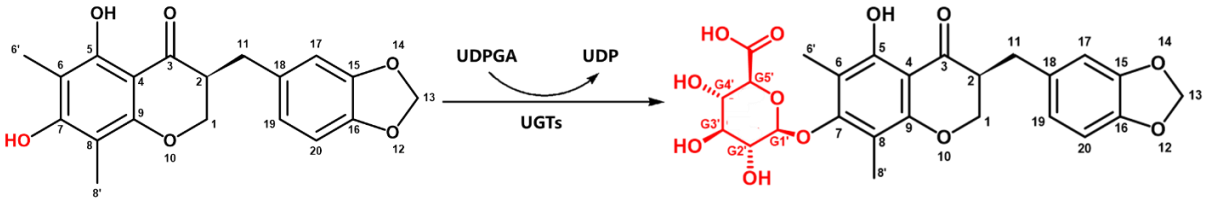

Figure 1. Chemical structures and proposed mechanism of MOA and its 7-*O*-glucuronide.

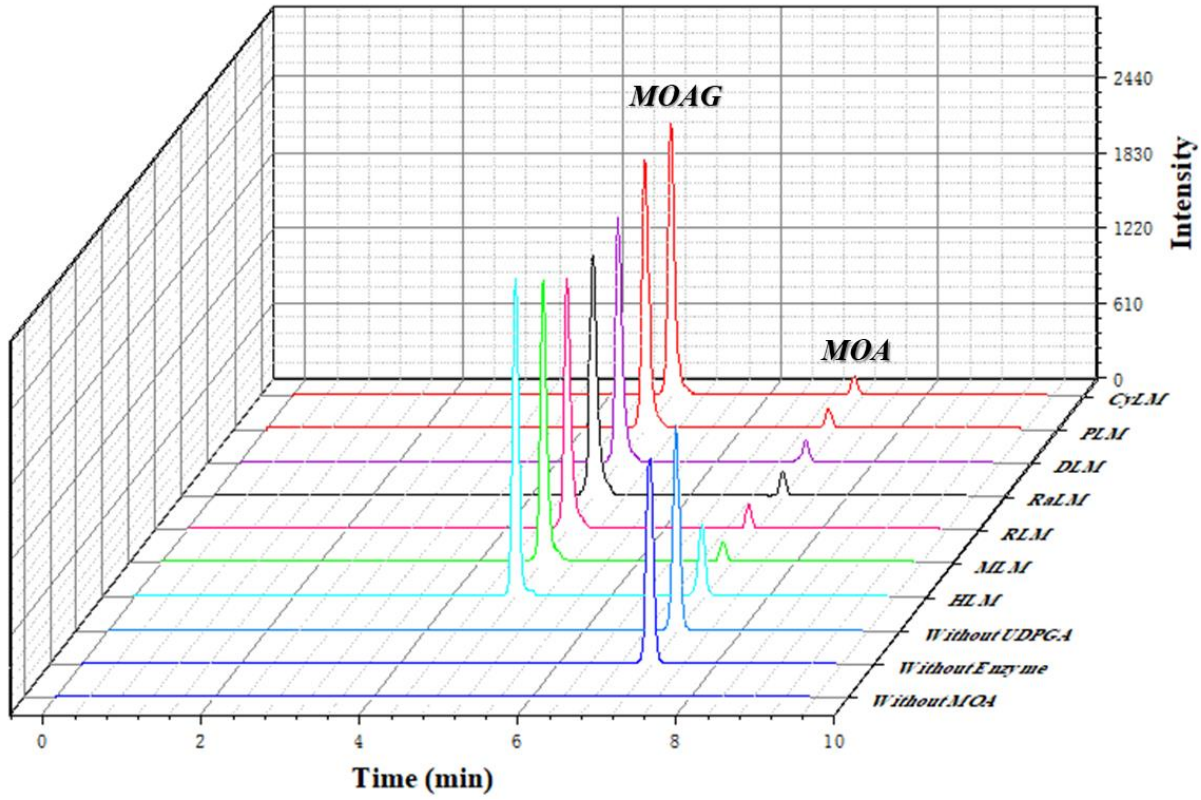

Figure 2. Representative LC-UV profiles of MOA (t_R = 6.74 min) and its 7-*O*-glucuronide (t_R = 4.74 min) in liver microsomes from different animal species and negative control (without UDPGA, enzyme or MOA).

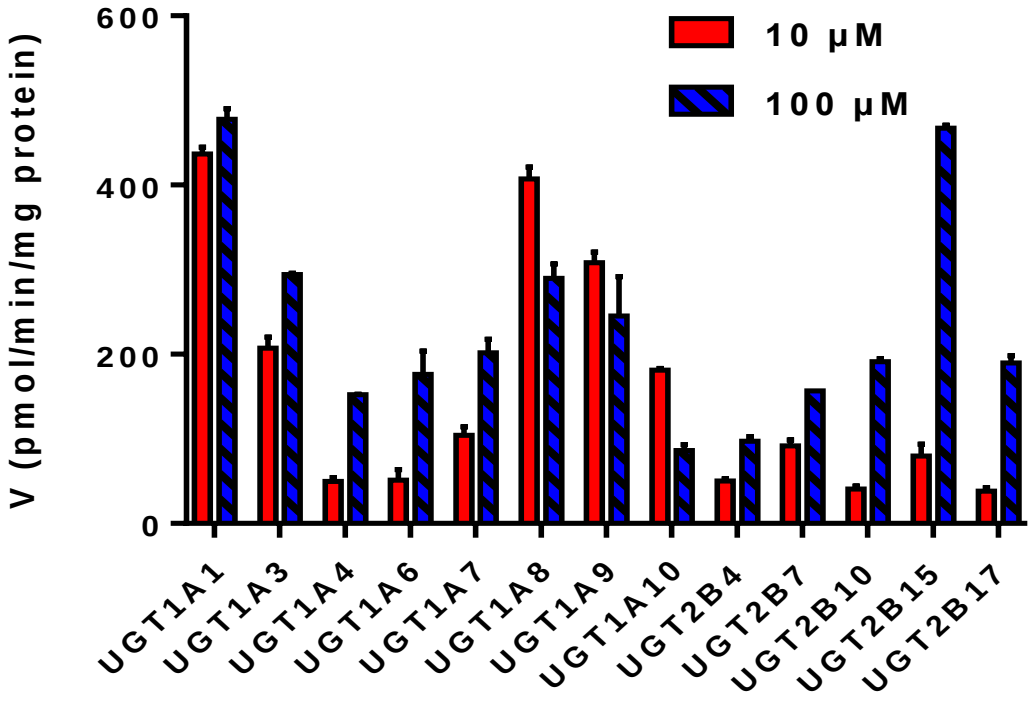

Figure 3. UGT reaction phenotyping assays of MOA 7-*O*-glucuronidation by using 13 various recombinant human UGT isoforms. Two substrate concentrations (10 µM & 100 µM) were used. Data expressed as mean ± SD (n=3).

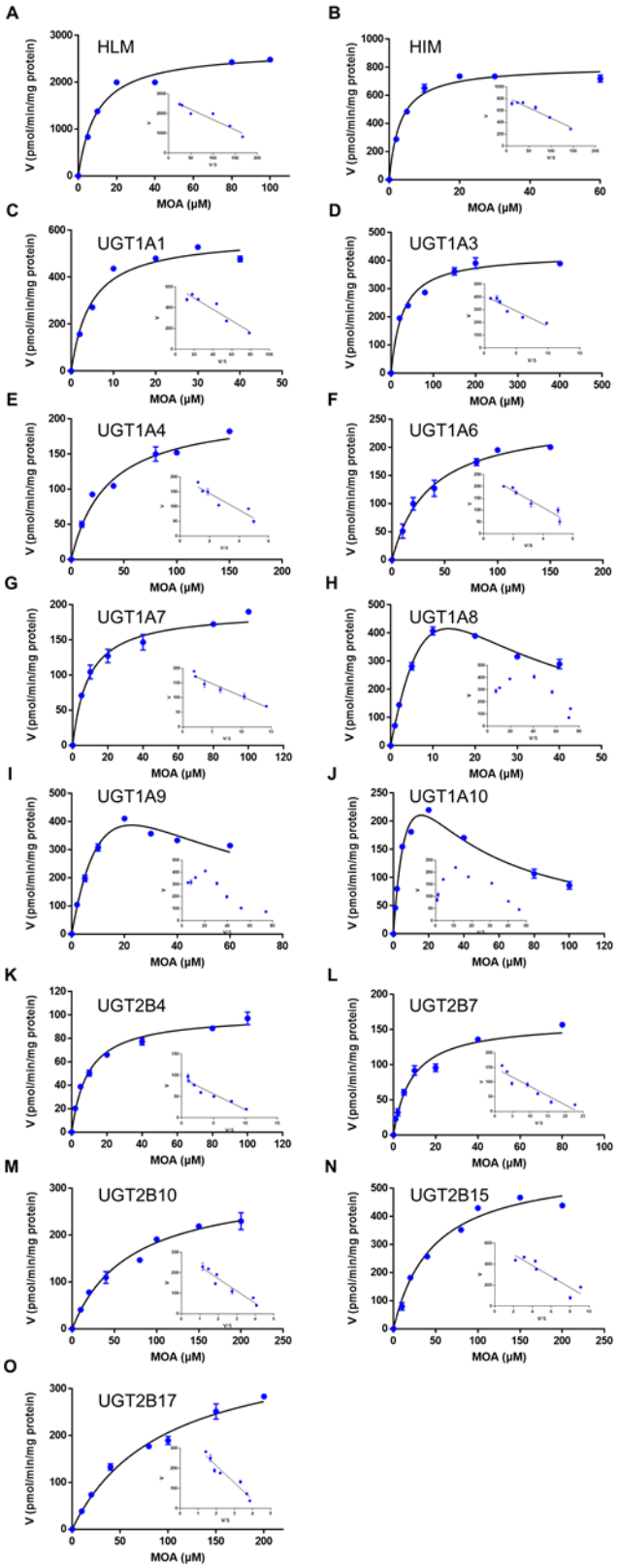

Figure 4. Enzymatic kinetics of MOA-7-*O*-glucuronidation in HLM (A), HIM (B) or recombinant human UGT1A1 (C), -1A3 (D), -1A4 (E), -1A6 (F), -1A7 (G), -1A8 (H), -1A9 (I), -1A10 (J), -2B4 (K), -2B7 (L), 2B10 (M), -2B15 (N) and -2B17 (O). Eadie-Hofstee plots (V/S-V) are displayed as the insets. Data points represent the mean of triplicate independent determinations, while the error bars represent the calculated S.D.(n=3).

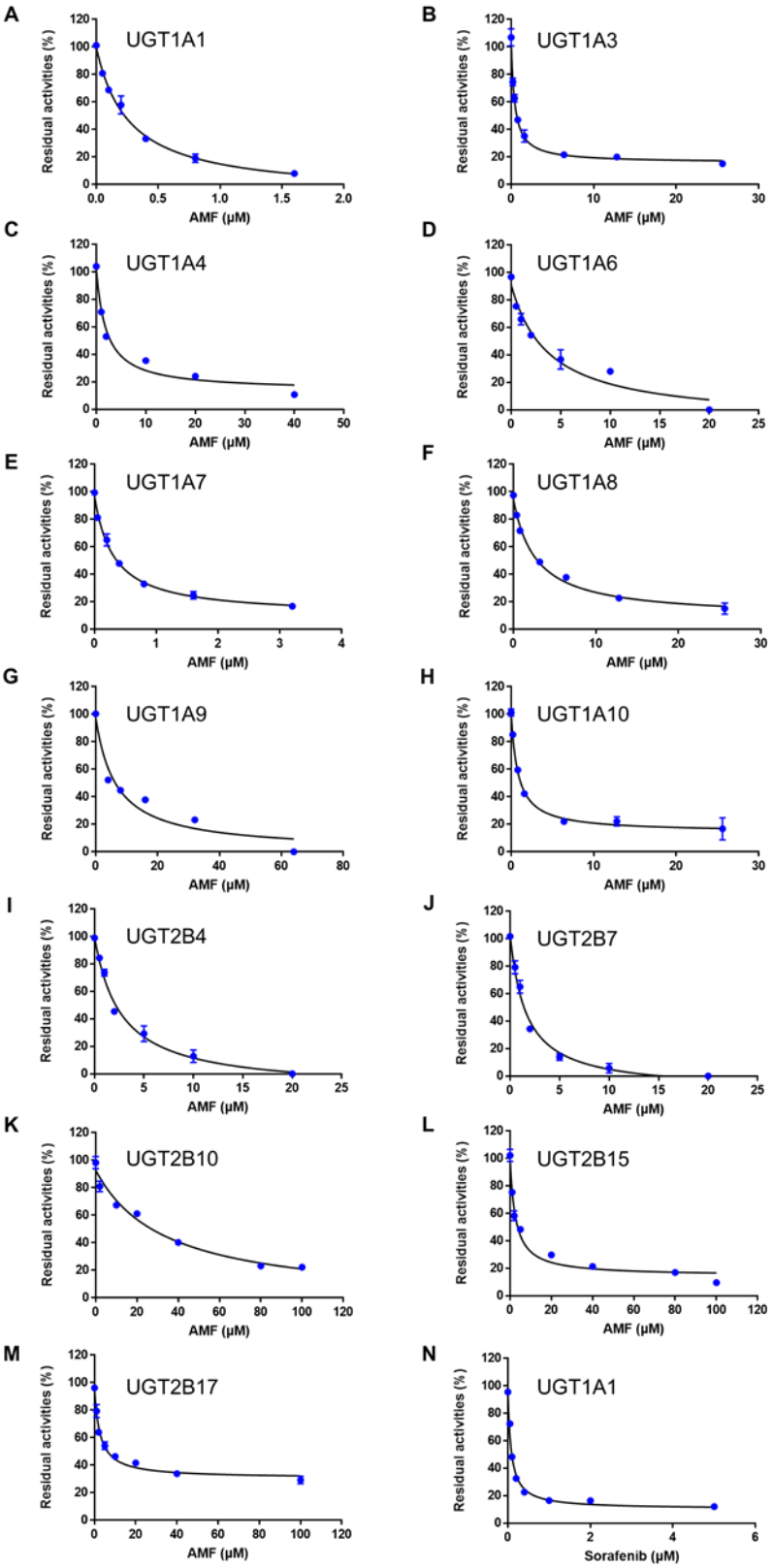

Figure 5. Dose-inhibition curves of amentoflavone against human UGT1A1 (A), -1A3 (B), -1A4 (C), -1A6 (D), -1A7 (E), -1A8 (F), -1A9 (G), -1A10 (H), -2B4 (I), -2B7 (J), -2B10 (K), -2B15 (L), -2B17 (M) and the positive control (sorafenib) against human UGT1A1-catalyzed MOA-7-*O*-glucuronidation. Data represent the mean ± SD (n=3).

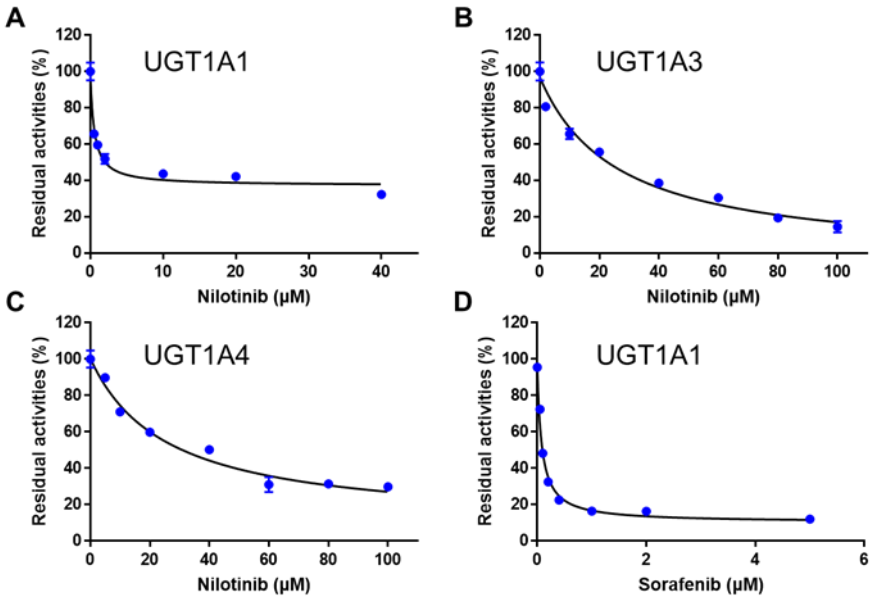

Figure 6. Dose-inhibition curves of nilotinib against human UGT1A1 (A), -1A3 (B), -1A4 (C) and the positive control (sorafenib) against human UGT1A1-catalyzed MOA-7-*O*-glucuronidation. Data represent the mean ± SD (n=3).

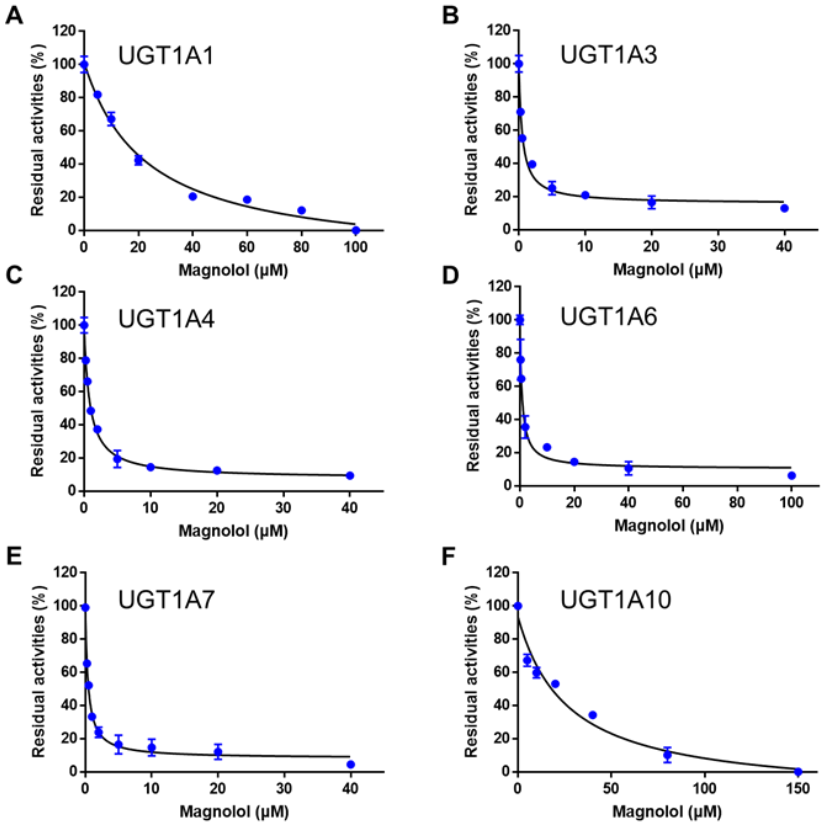

Figure 7. Dose-inhibition curves of magnolol against human UGT1A1 (A), -1A3 (B), -1A4 (C), -1A6 (D), -1A7 (E) and -1A10 (F) catalyzed MOA-7-*O*-glucuronidation. Data represent the mean ± SD (n=3).

Table 1. Assignment of the chemical shifts of each proton and carbon signals of MOA and its 7-*O*-glucuronide.

Position	MOA		MOA-7-*O*-G	
	δ^1H Mult (*J* in Hz)	**δ^{13}C**	**δ^1H Mult (*J* in Hz)**	**δ^{13}C**
1	4.10-4.31 (d, 7.1, 2H)	68.67	4.14-4.37 (d, 7,1, 2H)	68.7
2	4.9 s	47.6	4.87 s	46.9
3	--	198.41	--	199.9
4	--	103.37	--	104.0
5	--	157.7	--	157.7
6	--	101.3	--	110.22
7	--	159.2	--	158.8
8	--	102.3	--	111.69
9	--	162.2	--	161.1
11	2.69-3.12 (m, 2H)	32.25	2.68-3.13 (m, 2H)	32.17
13	5.94 s	100.85	5.94 s	100.87
15	--	147.91	--	147.92
16	--	146.37	--	146.42
17	6.72 (d, 1.7, 1H)	109.91	6.72 (d, 4.1, 1H)	108.94
18	--	132.03	--	131.78
19	6.76 s	121.85	6.75 s	121.88
20	6.78 s	107.76	6.79 s	107.73
6'8'-CH_3	2.0-2.01 (d, 5.7, 6H)	--	2.12-2.16 (d, 3.0, 6H)	
G1'	--	--	4.76 (d, 7.7, 1H)	104.48
G2'	--	--	3.58 (m, 1H)	71.8
G3'	--	--	3.60 (d, 9.6, 1H)	75.5
G4'	--	--	3.49 (d, 8.6, 1H)	73.9
G5'	--	--	3.65 (m, 1H)	75.9
COOH	--	--	--	161.1

Table 2. Kinetic parameters for MOA-7-*O*-glucuronidation in HLM, HIM and 13 recombinant human UGT enzymes.

Enzyme source	V_{max} (pmol/min/mg protein)	K_m (S_{50}) (μM)	V_{max}/K_m (μL/min/mg protein)	K_{si} (μM)	Kinetic mode
HLM	2690 ± 88.42	9.63 ± 1.17	279.33	--	Michaelis-Menten
HIM	808.2 ± 19.94	3.14 ± 0.36	257.39	--	Michaelis-Menten
UGT1A1	575.0 ± 26.35	4.69 ± 0.77	122.60	--	Michaelis-Menten
UGT1A3	423.8 ± 10.75	27.22 ± 3.01	15.57	--	Michaelis-Menten
UGT1A4	211.1 ± 11.35	34.11 ± 5.34	6.19	--	Michaelis-Menten
UGT1A6	252.3 ± 13.58	35.32 ± 5.03	7.14	--	Michaelis-Menten
UGT1A7	191.6 ± 6.31	9.10 ± 1.13	21.05	--	Michaelis-Menten
UGT1A8	2664 ± 694.4	27.33 ± 10.96	97.48	4.80	Substrate Inhibition
UGT1A9	1044 ± 289.7	20.68 ± 7.60	50.48	25.16	Substrate Inhibition
UGT1A10	488.4 ± 64.19	10.37 ± 2.14	47.1	23.88	Substrate Inhibition
UGT2B4	100.2 ± 2.43	9.28 ± 0.86	10.80	--	Michaelis-Menten
UGT2B7	161.1 ± 9.37	8.72 ± 1.45	18.47	--	Michaelis-Menten
UGT2B10	310.8 ± 16.42	68.77 ± 8.94	4.52	--	Michaelis-Menten
UGT2B15	583.2 ± 27.99	46.48 ± 6.85	12.55	--	Michaelis-Menten
UGT2B17	264.2 ± 15.16	94.99 ± 13.69	2.78	--	Michaelis-Menten

Table 3. The linear range, LOD, intra- and inter-day variability of the LC-UV based assay for quantitative determination of MOA and MOAG.

Compound	LOD (ng)	LOQ (ng)	Linear (ng)	Theoretical concentrations (ng)	Intra-day (n = 3)		Inter-day (n = 3)	
					Measured concentration (ng)	RSD (%)	Measured concentration (ng)	RSD (%)
MOA	0.09	0.45	0.09-855.86	3.42	3.46	0.8	3.45	0.7
MOAG	0.11	0.42	0.11-1295.86	0.52	0.50	1.0	0.49	1.5

Table 4. IC_{50} values of four known UGT inhibitors against 13 human UGTs by using MOA as the substrate.

Enzyme	IC_{50} (μM)			
	Amentoflavone	**Nilotinib**	**Magnolol**	**Fluconazole**
UGT1A1	0.26 ± 0.04	0.52 ± 0.03	22.66 ± 3.20	--
UGT1A3	0.41 ± 0.03	26.24 ± 0.03	0.54 ± 0.08	--
UGT1A4	1.99 ± 0.52	25.63 ± 4.90	0.85 ± 0.06	--
UGT1A6	3.78 ± 1.20	--	0.79 ± 0.13	--
UGT1A7	0.31 ± 0.03	--	--	--
UGT1A8	2.69 ± 0.35	--	--	--
UGT1A9	5.66 ± 1.78	--	0.42 ± 0.05	--
UGT1A10	0.81 ± 0.09	--	29.92 ± 5.59	--
UGT2B4	2.65 ± 0.40	--	--	--
UGT2B7	1.60 ± 0.21	--	--	96.63 ± 25.72
UGT2B10	37.4 ± 7.15	--	--	--
UGT2B15	2.61 ± 0.40	--	--	--
UGT2B17	2.68 ± 0.37	--	--	--

--: No inhibition or very weak inhibition (IC_{50} >100 μM)

Credit author statement

Qi-Hang Zhou and Wei-Wei Qin: Data curation, Writing - Original draft; Moshe Finel, Qing-Qing He, Dong-Zhu Tu, Chao-Ran Wang: Software, Validation, Investigation, Supervision; Guang-Bo Ge: Conceptualization, Methodology; Writing - Review and Editing.